CHEMISTRY
A EUROPEAN JOURNAL

DOI: 10.1002/chem.200801064

Mixed-Ligand Metal–Organic Frameworks with Large Pores: Gas Sorption Properties and Single-Crystal-to-Single-Crystal Transformation on Guest Exchange

Hye Jeong Park and Myunghyun Paik Suh*[a]

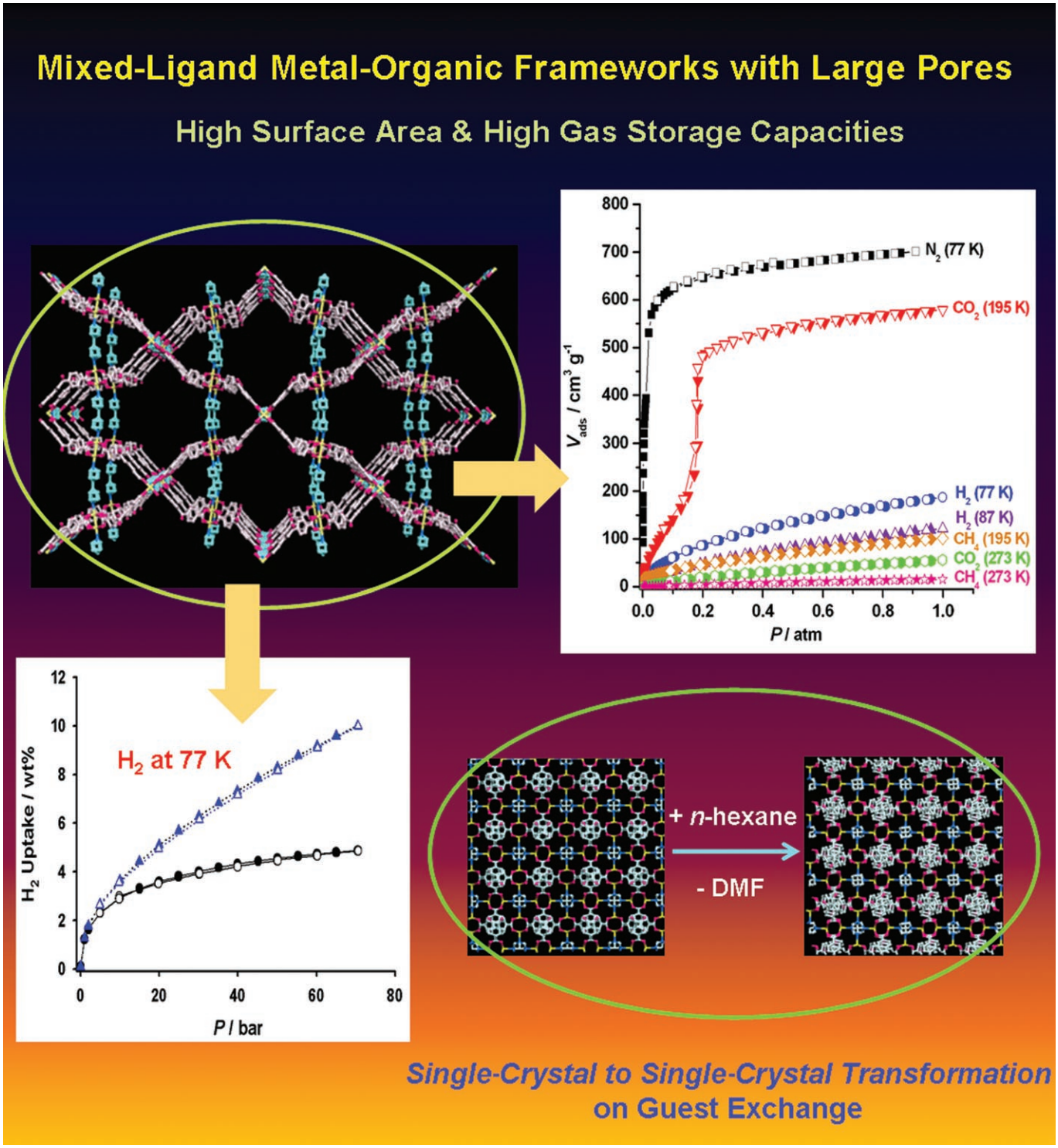

Abstract: Two isomorphous 3D metal–organic frameworks, $\{[Cu_2(BPnDC)_2(bpy)]\cdot 8DMF\cdot 6H_2O\}_n$ (**1**) and $\{[Zn_2(BPnDC)_2(dabco)]\cdot 13DMF\cdot 3H_2O\}_n$ (**2**), have been prepared by the solvothermal reactions of benzophenone 4,4′-dicarboxylic acid (H_2BPnDC) with $Cu(NO_3)_2\cdot 2.5H_2O$ and 4,4′-bipyridine (bpy), and with $Zn(NO_3)_2\cdot 6H_2O$ and 4-diazabicyclo[2.2.2]octane (dabco), respectively. Compounds **1** and **2** are composed of paddle-wheel $\{M_2(O_2CR)_4\}$ cluster units, and they generate 2D channels with two different large pores (effective size of larger pore: 18.2 Å for **1**, 11.4 Å for **2**). The framework structure of desolvated solid, $[Cu_2(BPnDC)_2(bpy)]_n$ (**SNU-6**; SNU = Seoul National University), is the same as that of **1**, as evidenced by powder X-ray diffraction patterns. **SNU-6** exhibits high permanent porosity ($1.05\,cm^3g^{-1}$) with high Langmuir surface area ($2910\,m^2g^{-1}$). It shows high H_2 gas storage capacity (1.68 wt% at 77 K and 1 atm; 4.87 wt% (excess) and 10.0 wt% (total) at 77 K and 70 bar) with high isosteric heat ($7.74\,kJ\,mol^{-1}$) of H_2 adsorption as well as high CO_2 adsorption capability (113.8 wt% at 195 K and 1 atm). Compound **2** undergoes a single-crystal-to-single-crystal transformation on guest exchange with *n*-hexane to provide $\{[Zn_2(BPnDC)_2(dabco)]\cdot 6(n\text{-hexane})\cdot 3H_2O\}_n$ ($\mathbf{2}_{hexane}$). The transformation involves dynamic motion of the molecular components in the crystal, mainly a bending motion of the square planes of the paddle-wheel units resulting from rotational rearrangement of phenyl rings and carboxylate planes of $BPnDC^{2-}$.

Keywords: adsorption · guest exchange · hydrogen storage · metal–organic frameworks · microporous materials

Introduction

Metal–organic frameworks (MOFs) with well-defined channels or pores have attracted great attention because of their potential for application in gas separation,[1–8] gas storage,[9–13] ion exchange,[14–17] and sensor technology.[18,19] The design of MOFs as functional materials can be achieved by selecting proper metal and organic building blocks. In particular, the concept of secondary building units (SBUs) with specific geometry is useful in obtaining the rationally designed MOFs because it significantly improves the predictability of molecular architectures.[20,21] Among various functions of porous MOFs, hydrogen storage has been the center of interest because of the needs for an alternative fuel in mobile applications. The U.S. Department of Energy has set the target to develop a material that can store 6.0 wt% or $45\,gL^{-1}$ of H_2 gas at ambient temperature by the year 2010.[22] In addition, the selective adsorption of CO_2 from a gaseous mixture is important because CO_2 gas is a major source of greenhouse gas emissions. The highest H_2 gas uptake data reported so far is 7.5 wt% at 77 K and 70 bar in MOF-177,[23] but the best room temperature storage data are far less than 1% (0.62 wt%).[24] The highest CO_2 uptake data reported so far is 147 wt% at 298 K and 35 bar in MOF-177.[25] Recently, flexible and dynamic MOFs that change their structures in response to external stimuli with retention of single crystallinity[4,12,26–34] have attracted growing interest since they are important for the development of certain devices and sensors.

Here, we report two isomorphous 3D metal–organic frameworks, $\{[Cu_2(BPnDC)_2(bpy)]\cdot 8DMF\cdot 6H_2O\}_n$ (**1**) and $\{[Zn_2(BPnDC)_2(dabco)]\cdot 13DMF\cdot 3H_2O\}_n$ (**2**), which have been prepared by the solvothermal reactions of benzophenone 4,4′-dicarboxylic acid (H_2BPnDC) with $Cu(NO_3)_2\cdot 2.5H_2O$ and 4,4′-bipyridine (bpy), and with $Zn(NO_3)_2\cdot 6H_2O$ and 4-diazabicyclo[2.2.2]octane (dabco), respectively. Compounds **1** and **2** form non-interpenetrating 3D frameworks despite the fact that they have large free spaces (83.7% for **1** and 74.5% for **2** of the total volume) and large effective pore sizes (18.2 Å in **1** and 11.4 Å in **2**). Desolvated solid $[Cu_2(BPnDC)_2(bpy)]_n$ (**SNU-6**), which has the same framework structure as **1** as evidenced by the powder X-ray diffraction (PXRD) patterns, exhibits high permanent porosity ($1.05\,cm^3g^{-1}$) with high surface area (Langmuir, $2910\,m^2g^{-1}$), high H_2 storage capacity (1.68 wt% at 77 K and 1 atm; 4.87 wt% (excess) and 10.0 wt% (total) at 77 K and 70 bar) with high isosteric heat ($7.74\,kJ\,mol^{-1}$), and high CO_2 adsorption capacity (113.8 wt% at 195 K and 1 atm) with an unusual S-shaped isotherm. Compound **2** undergoes a single-crystal-to-single-crystal transformation on exchange of the DMF guest molecules with hexane to form $\{[Zn_2(BPnDC)_2(dabco)]\cdot 6(n\text{-hexane})\cdot 3H_2O\}_n$ ($\mathbf{2}_{hexane}$). The X-ray structure of $\mathbf{2}_{hexane}$ reveals bending of the square planes of the paddle-wheel units, which result from rotation-

[a] H. J. Park, Prof. M. P. Suh
Department of Chemistry
Seoul National University
Seoul 151-747 (Republic of Korea)
Fax: (+82) 2-886-8516
E-mail: mpsuh@snu.ac.kr

Supporting information for this article is available on the WWW under http://dx.doi.org/10.1002/chem.200801064.

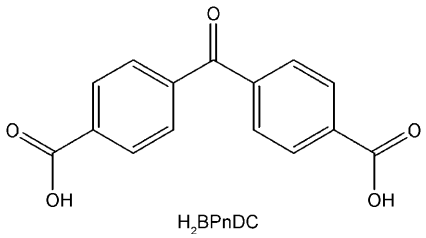

al rearrangement of phenyl rings and carboxylate planes of $BPnDC^{2-}$.

Results and Discussion

X-ray structure and properties of $\{[Cu_2(BPnDC)_2(bpy)]\cdot 8DMF\cdot 6H_2O\}_n$ (1): Blue truncated octahedral crystals of **1** were prepared by heating a solution of $Cu(NO_3)_2\cdot 2.5H_2O$, H_2BPnDC, and 4,4′-bipyridine in DMF/EtOH at 80 °C for 24 h. The single-crystal X-ray structure of **1** (Figure 1) shows a non-interpenetrating 3D coordination network, which is different from the previously reported ones resulting from hydrothermal reactions.[35,36]

In **1**, Cu^{II} shows a square-pyramidal coordination geometry by being coordinated with four oxygen atoms of four different $BPnDC^{2-}$ ligands at the equatorial sites and a nitrogen atom of 4,4′-bpy at the axial position. The $Cu-O_{BPnDC}$ bond lengths are 1.974(2) Å (average) and the $Cu-N_{bpy}$ bond length is 2.161(4) Å. $BPnDC^{2-}$ is a bis-bidentate ligand, and coordinates four different Cu^{II} centers. Each carboxylate group of four $BPnDC^{2-}$ moieties links two Cu^{II} centers, with the Cu^{II}–Cu^{II} distance of 2.669(1) Å, to form a paddle-wheel SBU. The $BPnDC^{2-}$ is a bent linker and the dihedral angle between the two phenyl rings is 67.69(14)°.

In general, 2D layers are assembled from paddle-wheel binuclear M_2 units and dicarboxylate linkers, and 3D primitive cubic MOFs can be constructed by linking the 2D layers with diamine pillars.[21] In our independent experiments, the solvothermal reactions of $Cu(NO_3)_2\cdot 2.5H_2O$ and H_2BPnDC in DEF/EtOH (DEF = N,N′-diethylformamide) or in DMA afforded 2D networks in which paddle-wheel binuclear Cu_2 units were bridged by $BPnDC^{2-}$.[37] Therefore, we expected that these types of 2D layers would be further linked by a 4,4′-bpy pillar to construct a 3D framework.

In **1**, however, Cu_2 paddle-wheel SBUs bridged by $BPnDC^{2-}$ form a 3D framework by themselves without a pillar because the dihedral angles between the neighboring square planes formed by the carboxylate carbon atoms of the paddle-wheel units are 90.00(0)° (Figure 1c). The 4,4′-bpy ligands, which link the paddle-wheel units located linearly, significantly affect the paddle-wheel positions in **1** (Figure 1d). As shown in Figure 1c, eight square planes (S1–S8) formed by the carboxylate carbon atoms of paddle-wheel

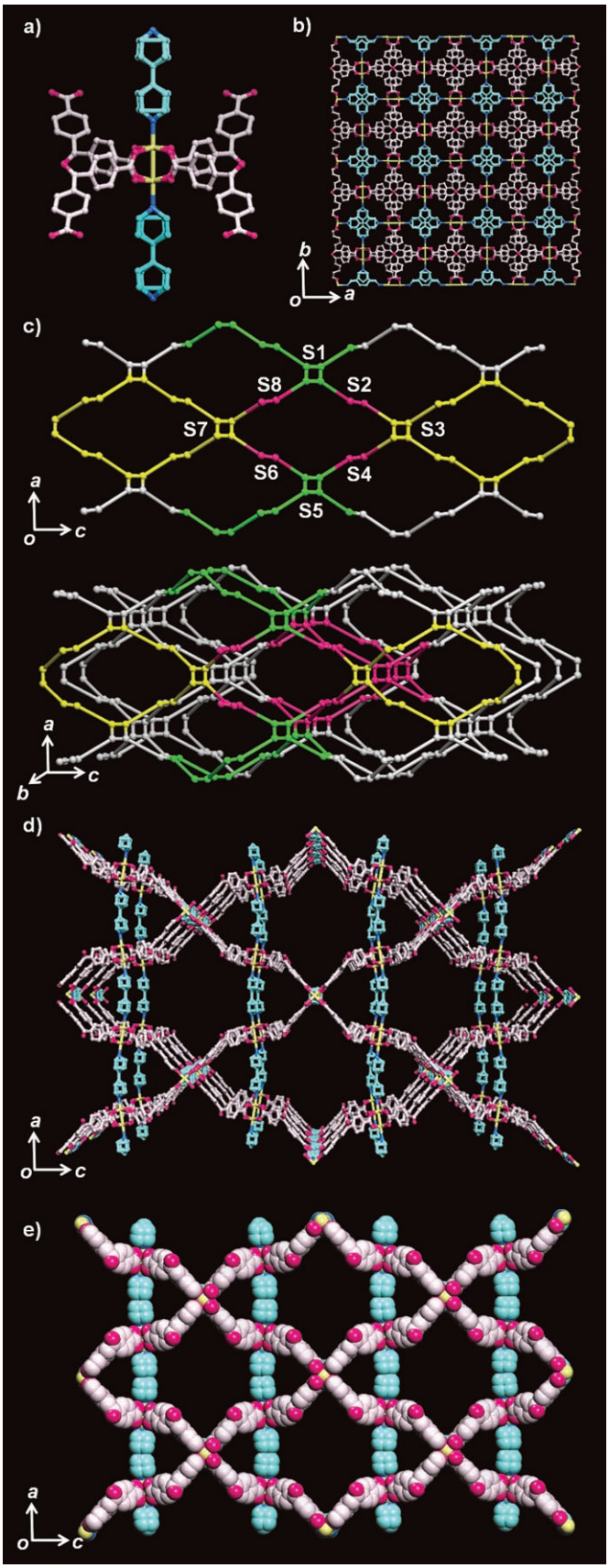

Figure 1. X-ray crystal structure of **1**. a) The coordination geometry of the paddle-wheel $\{Cu_2(BPnDC)_2(bpy)\}$ unit. 4,4′-bpy is rotationally disordered twofold. H atoms are omitted for clarity. Color scheme: Cu, yellow; N, blue; O, dark pink; C, pale pink; C in 4,4′-bpy, pale blue. b) A view showing an arrangement of paddle-wheel SBUs in the framework. They are positioned with the dihedral angle of 90.00(0)° between the neighboring paddle-wheel square planes. c) A view showing how the paddle-wheel SBUs are located to construct the 3D network $\{Cu_2(BPnDC)_2\}$ by themselves. Paddle-wheel square planes of (S1 and S5), (S2, S4, S6, and S8), and (S3 and S7) are extended along the *a* (green), *b* (dark pink), and *c* axis (yellow), respectively. d) A perspective view showing how 4,4′-bpy linkers connect paddle-wheel units of the network in c. e) A space-filling model (CPK) view showing the two kinds of channels.

SBUs make a rhombus, in which the square planes lie alternately along the *ac* and the *bc* plane with the dihedral angle of 90.00(0)°. Sets of square planes, (S1 and S5), (S2, S4, S6, and S8), and (S3 and S7) are extended along the *a*, *b*, and *c* axes, respectively. Parallel squares such as (S2 and S4) and (S6 and S8) are connected by 4,4′-bpy linkers to generate two kinds of channels having a triangular and a hexagonal aperture, which gives rise to the Kagome nets (Figure 1d and e).[38,39] The edge length and the effective size of the small triangular channel are 10.7 and 5.6 Å, respectively. The large hexagonal channel has a width of 21.6 Å as measured between the centers of two opposite phenyl rings of $BPnDC^{2-}$, and it becomes 18.2 Å when the van der Waals surface is considered. Framework **1** generates 2D channels in the [100] and [010] directions.

The solvent-accessible volume estimated by PLATON[40] is as high as 83.7%, 2.65 $cm^3 g^{-1}$. The calculated density of **1** after solvent removal is as low as 0.316 $g cm^{-3}$, which is comparable to that of mesoMOF-1 (0.262 gcm^{-3}).[41] The guest molecules inside the pores could not be refined owing to the severe disorder, as common to microporous MOFs with large pores. Therefore, the identity and number of the guest molecules (8 DMF and 6 H_2O) in **1** were determined on the basis of IR spectra, elemental analysis, and thermogravimetric analysis (TGA) data. The final structural model was refined without the guest molecules by using the SQUEEZE option of PLATON.[40] The TGA data for framework **1** measured under an N_2 atmosphere indicated that crystal **1** lost solvent guest molecules as soon as it was removed from the mother liquor. It lost 44.0% weight (calcd. 45.8%) upon heating to approximately 100 °C. The TGA and PXRD data measured at various temperatures suggest that **1** is thermally stable up to 230 °C (see the Supporting Information).

When **1** was heated in a Schlenk tube at 100 °C under vacuum for 2 h, desolvated solid $[Cu_2(BPnDC)_2(bpy)]_n$ (**SNU-6**) resulted, which was characterized by elemental analysis, FTIR spectra, TGA data, and PXRD data. In Figure 2, PXRD patterns of **1** and its desolvated solid **SNU-6** are compared. The measured PXRD pattern of **1** is almost coincident with that of the simulated pattern derived from the X-ray single-crystal raw data, showing that the bulk sample is the same as the single crystal, but it is a little different from the simulated pattern when electron densities corresponding to the disordered guest molecules are ignored by using the SQUEEZE option of PLATON.[40] The PXRD pattern of the desolvated solid **SNU-6** is same as the simulated pattern based on the squeezed single-crystal X-ray data of **1**, which indicates that the framework structure of **1** is retained in **SNU-6**. When **SNU-6** is exposed to DMF vapor for three days, the PXRD pattern of **1** is regenerated, thus indicating that guest molecules are reintroduced to the framework. The elemental analysis data for the resolvated sample indicates that seven DMF and four water molecules are included per formula unit of the solid (elemental analysis calcd (%) for $\{[Cu_2(BPnDC)_2(bpy)]\cdot 7DMF\cdot 4H_2O\}_n$: C 51.54, H 5.89, N 8.87; found: C 52.19, H 5.61, N 9.05).

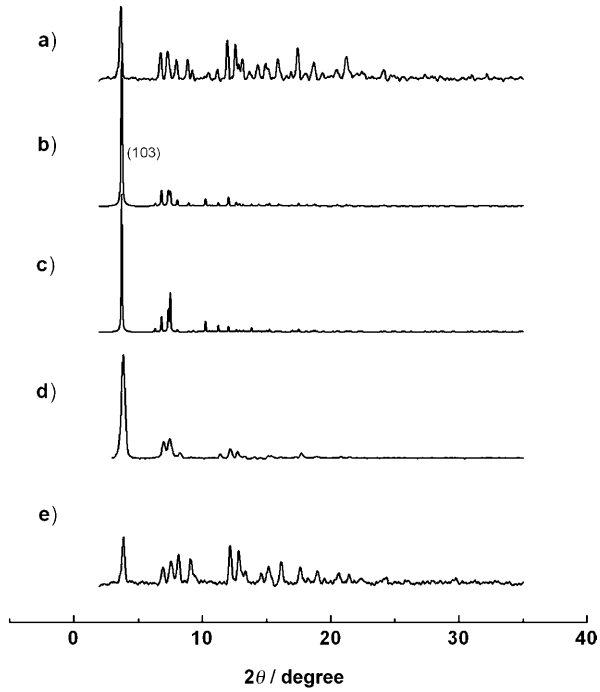

Figure 2. The PXRD patterns for **1** and its desolvated solid **SNU-6**. a) **1** as synthesized. b) Simulated pattern based on the single-crystal X-ray raw data of **1**. c) Simulated pattern from the single-crystal X-ray data of **1**, in which electron densities corresponding to the disordered guest molecules are flattened by using the SQUEEZE option of PLATON.[40] d) **SNU-6** that was prepared by drying **1** at 100 °C under vacuum for 2 h. e) Solid isolated after exposure of **SNU-6** to DMF vapor for 3 d.

Gas sorption properties of $[Cu_2(BPnDC)_2(bpy)]_n$ (SNU-6): To examine the porosity of **SNU-6**, gas sorption capacities were measured for N_2, H_2, CO_2, and CH_4 gases, and the data are presented in Table 1.

Table 1. Gas adsorption data of **SNU-6**.

Gas	*T* [K]	Surface area $[m^2 g^{-1}]$[a,b]	Pore volume $[cm^3 g^{-1}]$	mmol gas per g host	wt% gas[c]	Gas adsorbed per volume host[d] $[g L^{-1}]$
N_2	77	2910,[a] 2590[b]	1.05	31.3	87.7	277
H_2	77	–	–	8.35	1.68	5.31
		–	–	24.2[e]	4.87[e]	15.4[e]
		–	–	49.6[f]	10.0[f]	31.6[f]
H_2	87	–	–	5.43	1.10	3.48
CO_2	195	–	–	25.8	113.8	360
CO_2	273	–	–	2.50	11.0	34.8
CH_4	195	–	–	4.53	7.26	23.1
CH_4	273	–	–	0.69	1.11	3.50

[a] Langmuir surface area. [b] BET surface area. [c] Amount of gas adsorbed at $P = 690$ Torr for N_2 and at $P = 760$ Torr for all other gases. [d] The values are calculated by (mass of adsorbed gas [g]) × (density of sample = 316 $g L^{-1}$), assuming that the cell volume of **1** is retained in its desolvated solid (**SNU-6**). [e] Excess adsorption capacity at 77 K and 70 bar. [f] Total adsorption capacity at 77 K and 70 bar.

The N_2 sorption isotherm shows typical Type-I sorption behavior, indicating the permanent microporosity (Figure 3). The Brunauer–Emmett–Teller (BET) and Langmuir surface area are 2590 and 2910 $m^2 g^{-1}$, respectively, which are com-

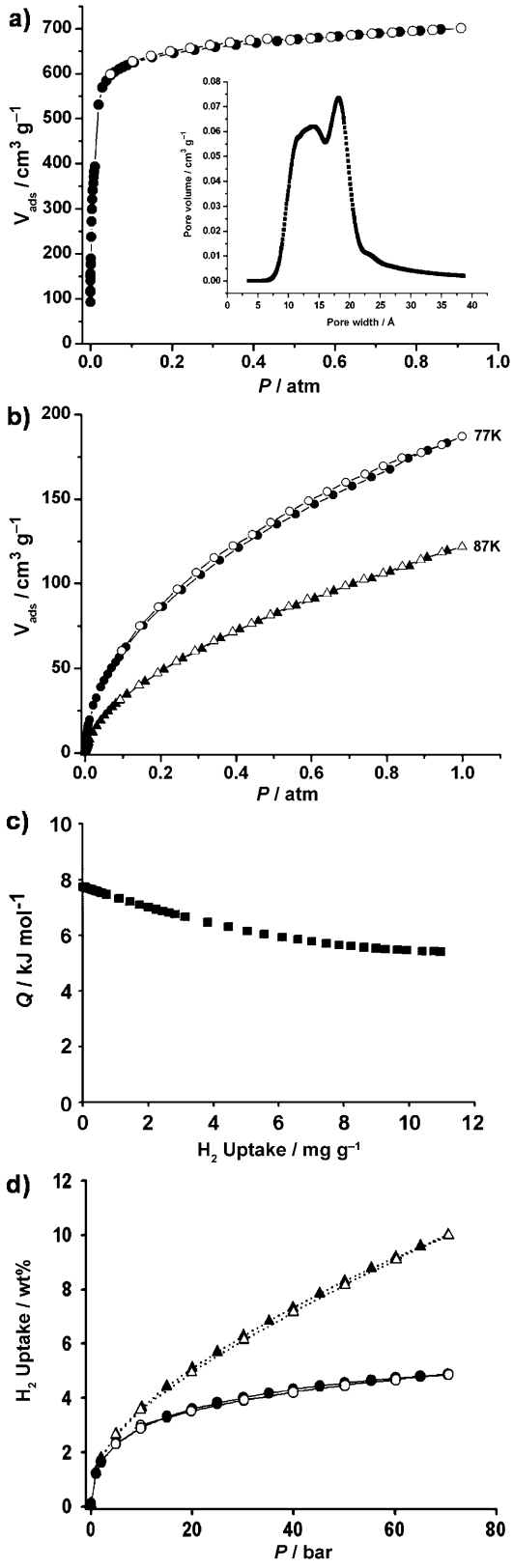

Figure 3. N_2 and H_2 gas sorption isotherms for **SNU-6**. a) N_2 at 77 K; $P_o(N_2) = 804.00$ Torr; the inset shows the pore size distributions. b) H_2 at 77 K (circle) and 87 K (triangle). c) Isosteric heat of H_2 adsorption. d) Excess (circle) and total (triangle) H_2 adsorption at 77 K and high pressures. Filled shapes: adsorption. Open shapes: desorption.

parable to that of IRMOF-1 (2833 $m^2 g^{-1}$).[25] The pore volume estimated by applying the Dubinin–Radushkevich equation is 1.05 $cm^3 g^{-1}$. The plot of pore size distribution based on the Saito–Foley model[42] indicates that pore diameters of **SNU-6** are 14.0 and 18.2 Å, coincident with that estimated from the X-ray structure of **1** (18.2 Å). It should be noted that surface area and pore volume of **SNU-6** derived from N_2 adsorption data are much lower than those estimated from the X-ray crystal structure of **1** (surface area, 3980 $m^2 g^{-1}$; pore volume, 2.66 $cm^3 g^{-1}$) by using the Materials Studio program[43] with a probe radius of 1.82 Å, which is appropriate for N_2, and a grid interval of 0.25 Å.

Solid **SNU-6** adsorbs H_2 gas up to 1.68 wt% (5.31 $g L^{-1}$) at 77 K and 1 atm (187 $cm^3 g^{-1}$ at STP, 6.85 H_2 molecules per formula unit), and 1.10 wt% at 87 K and 1 atm (122 $cm^3 g^{-1}$ at STP, 4.45 H_2 molecules per formula unit). The H_2 adsorption capacity is relatively good, and comparable to that of $[Zn_2(bpy)(tmbdc)_2]$ (1.68 wt% at 78 K and 1 atm)[21] (tmbdc = tetramethyl terephthalate). The isosteric heat of H_2 adsorption for **SNU-6** is 7.74–5.41 kJ mol^{-1} depending on the degree of H_2 loading (Figure 3), as estimated from the H_2 isotherms at 77 and 87 K by using the virial equation.[11,44] The zero coverage isosteric heat (7.74 kJ mol^{-1}) is comparable to that of the desolvated solid of $Cu_3[(Cu_4Cl)_3(TPB\text{-}3tz)_8]_2 \cdot 11\,CuCl_2 \cdot 8\,H_2O \cdot 120\,DMF$ (8.2 kJ mol^{-1}; TPB-3tz = 1,3,5-tri-*p*-(tetrazol-5-yl)phenylbenzene).[45] On exposure of the sample to air for three days, the H_2 adsorption capacity was reduced even after the reactivation (162 $cm^3 g^{-1}$ at STP, 1.46 wt% at 77 K and 1 atm). It has been reported that H_2 adsorption capacities of some MOF materials depend on the degree of exposure to air.[9]

When H_2 pressure is increased up to 70 bar at 77 K, **SNU-6** exhibits an excess H_2 adsorption of 4.87 wt% and total H_2 uptake of 10.0 wt%, in which the excess is the measured amount of physisorbed gas on the surface and the total is the sum of the amount of adsorbed gas on the surface plus the pressurized gas within the pores.[9,11] The excess H_2 adsorption is not yet saturated and still increasing even at 70 bar, similarly to the sorption behaviors of IRMOF-20[23] and MIL-101[10] although many other microporous MOFs show flattening around 40 bar.[23] The big difference between the excess and total H_2 uptake of **SNU-6** is attributed to the measured large pore volume (77.4%). The volumetric adsorption capacities (excess 15.4 $g L^{-1}$; total 31.6 $g L^{-1}$) are relatively low due to the low framework density (0.316 $g cm^{-3}$). At 298 K and 70 bar, H_2 adsorption capacity is 0.28 wt%, similarly to all other MOFs that show very low capacity, lower than 1%.

The CO_2 gas sorption isotherms of **SNU-6** measured at 195 and 273 K are shown in Figure 4. The CO_2 isotherm at 195 K shows a two-step adsorption with a little hysteresis. In an initial step, it adsorbs 37.3 wt% (8.5 $mmol g^{-1}$, 190 $cm^3 g^{-1}$ at STP) of CO_2 at 0.15 atm, and in the second step it uptakes up to 113.8 wt% (25.8 $mmol g^{-1}$, 579 $cm^3 g^{-1}$ at STP) at 0.15–1 atm region. The stepwise, hysteretic, pressure-dependent gas adsorption has been observed in several flexible and dynamic porous MOFs, which respond to specific guest

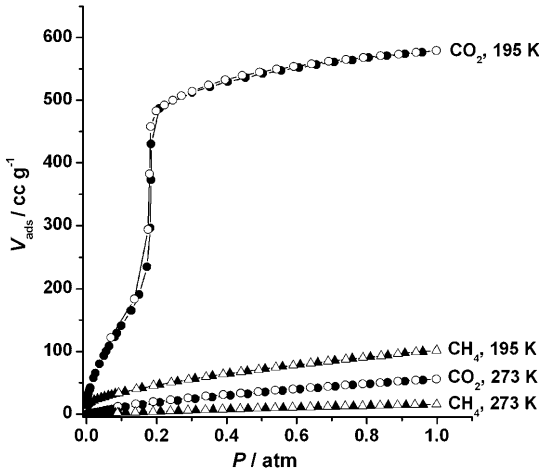

Figure 4. CO_2 (circle) and CH_4 (triangle) sorption isotherms for **SNU-6**. Filled shapes: adsorption. Open shapes: desorption.

molecules by means of a breathing or a gate-opening process.[46–51] Recently, Yaghi's group reported an S-shaped CO_2 isotherm for IRMOF-1 that is similar to the present case, and explained it by the attractive electrostatic interactions between CO_2 molecules.[52] The CO_2 adsorption capacity of **SNU-6** is superior to those for other MOFs measured under similar conditions. The highest uptake data under the same conditions that have been reported so far is 148.9 wt% in IRMOF-1.[52] The CO_2 storage capacity of **SNU-6** at 273 K and 1 atm is 11.0 wt% (2.5 mmolg^{-1}, 56.0 $cm^3 g^{-1}$ at STP), significantly lower than that measured at 195 K.

The CH_4 gas isotherms indicate that **SNU-6** can store up to 7.27 wt% (4.53 mmolg^{-1}, 101.5 $cm^3 g^{-1}$ at STP) of CH_4 at 195 K and 1 atm, and 1.11 wt% (0.69 mmolg^{-1}, 15.5 $cm^3 g^{-1}$ at STP) at 273 K and 1 atm. The big differences between CO_2 and CH_4 adsorption capacities of **SNU-6** can be applied in gas separation processes.

X-ray structure and properties of {[Zn_2(BPnDC)$_2$(dabco)]·13DMF·3H_2O}$_n$ (2): Colorless crystals of **2** were obtained by heating a solution of $Zn(NO_3)_2$·6H_2O, H_2BPnDC, and 4-diazabicyclo[2.2.2]octane (dabco) in DMF at 100 °C for three days. The X-ray structure of **2** reveals a non-interpenetrating 3D coordination network that is similar to **1** (Figure 5). In **2**, a pair of Zn^{II} centers forms a {Zn_2(O_2CR)$_4$} paddle-wheel SBU unit, but nitrogen atoms of the dabco instead of those of 4,4′-bpy are coordinated at the axial sites of the Zn^{II} ions. The Zn^{II}–Zn^{II} distance (3.007(2) Å) suggests that there is no significant interaction between the Zn^{II} ions in a paddle-wheel SBU (the sum of the van der Waals radii of Zn^{II} is 2.80 Å).[53] The average Zn–O_{BPnDC} distance is 2.040(2) Å and the Zn–N_{dabco} distance is 2.038(5) Å. The dihedral angle between the two phenyl rings in $BPnDC^{2-}$ is 59.02(25)°, smaller than 67.69(14)° in **1**. The dihedral angle between the neighboring square units formed by the carboxylate carbon atoms of paddle-wheel SBUs is 89.97(1)°, and thus paddle-wheel SBUs linked by $BPnDC^{2-}$ construct a 3D framework. The axial sites of the

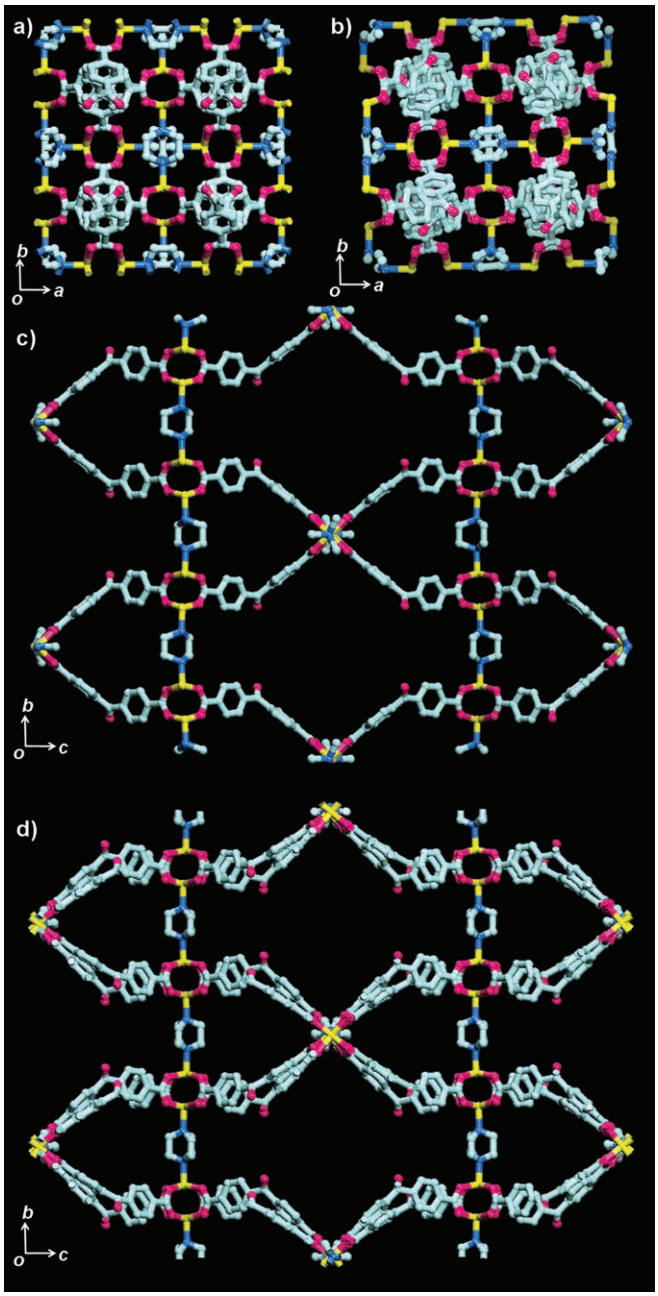

Figure 5. X-ray crystal structure of **2** and $\mathbf{2}_{hexane}$. Side view showing the arrangement of paddle-wheel SBUs in a) **2** and b) $\mathbf{2}_{hexane}$. Top view showing the two kinds of channels in c) **2** and d) $\mathbf{2}_{hexane}$. H atoms are omitted for clarity. Color scheme: Zn, yellow; N, blue; O, dark pink; C, pale blue.

paddle-wheel units run along the *a* and *b* axis and are occupied by nitrogen atoms of the dabco ligand.

Framework **2** generates two kinds of channels with triangular and hexagonal apertures (Figure 5). The edge length and the effective size of the small triangular channels are 8.0 and 3.9 Å, respectively. The large hexagonal channel has widths of 14.8 Å as measured between the closest C–C distance of two opposite phenyl rings of $BPnDC^{2-}$. When the van der Waals surface is considered, the effective width of the hexagonal window becomes 11.4 Å.

The solvent-accessible free volume of **2** is 74.5% of the total crystal volume, as estimated by PLATON.[40] The void space is filled with guest solvent molecules, but they could not be defined by the X-ray structure because of the severe disorder. Therefore, the identity and number of the guest molecules (13 DMF and 3 H_2O) in **2** were determined on the basis of IR spectra, elemental analysis, and TGA data. The final structural model was refined without the guest molecules by using the SQUEEZE option of PLATON.[40]

Framework **2** is insoluble in water and common organic solvents. Interestingly, it maintained the single crystallinity as well as transparency when a single crystal of **2** was immersed in organic solvents such as MeCN, MeOH, $CHCl_3$, toluene, benzene, acetone, hexane, and diethyl ether. TGA data shows that the as-synthesized material releases solvent molecules even at room temperature, and loses 52.4% weight on heating to 100 °C, which corresponds to the loss of 13 DMF and 3 H_2O molecules (calcd 56.3%). The variable-temperature PXRD pattern indicates that the framework structure of **2** can be maintained up to 360 °C (see the Supporting Information).

When **2** was heated in a Schlenk tube at 100 °C under vacuum for 2 h, desolvated solid $[Zn_2(BPnDC)_2(dabco)]_n$ (**2′**) resulted. As shown in Figure 6, the measured PXRD pattern of **2** is almost coincident with the simulated pattern

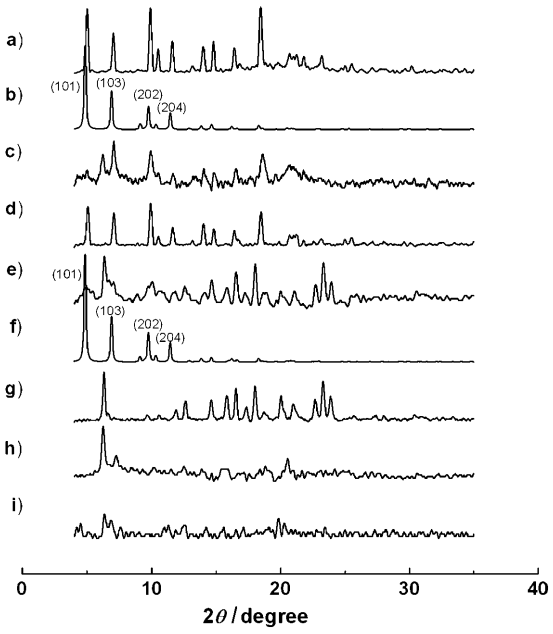

Figure 6. The PXRD patterns for a) **2** as synthesized, b) **2** simulated from the single-crystal X-ray data, in which electron densities corresponding to the disordered guest molecules are flattened by using the SQUEEZE option of PLATON,[40] c) **2′** prepared by drying **2** at 100 °C under vacuum for 2 h, d) solid isolated after exposure of **2′** to DMF vapor for 3 d, e) guest-exchanged solid, $\{[Zn_2(BPnDC)_2(dabco)]\cdot 6(n\text{-hexane})\cdot 3H_2O\}_n$ ($\mathbf{2}_{\mathbf{hexane}}$), f) $\mathbf{2}_{\mathbf{hexane}}$ simulated based on X-ray single-crystal data, in which electron densities corresponding to the disordered guest molecules are flattened by using the SQUEEZE option of PLATON,[40] g) a solid resulting after exposure of $\mathbf{2}_{\mathbf{hexane}}$ to air for 5 min, h) a solid prepared by drying $\mathbf{2}_{\mathbf{hexane}}$ at 150 °C under vacuum for 2 h, i) a solid isolated after immersion of the sample in (h) in *n*-hexane for 2 days.

derived from the X-ray single-crystal data, which indicates that the bulk sample is the same as the single crystal. The small differences in the relative intensities between the measured and the simulated patterns are attributed to the fact that the measured sample contains guest molecules, whereas the simulated pattern ignored the guests by applying the SQUEEZE option of PLATON.[40] The PXRD pattern of the desolvated solid **2′** is different from that of **2**, which indicates that the framework structure changes on removal of the guest molecules. However, the PXRD pattern of **2** was regenerated when **2′** was exposed to DMF vapor for three days, thus indicating that the original structure was restored on reintroduction of the guest molecules. The elemental analysis data for the resolvated solid indicated that twelve DMF and six water molecules per formula unit were included in the solid (elemental analysis calcd (%) for $\{[Zn_2(BPnDC)_2(dabco)]\cdot 12DMF\cdot 6H_2O\}_n$: C 49.01, H 7.08, N 11.11; found: C 49.24, H 7.01, N 11.06). Contrary to **SNU-6**, solid **2′** did not adsorb N_2 or H_2 gas, indicating that the material becomes nonporous on removal of the guests. The differences in metal ion and type of pillars linking the paddlewheel units greatly affect the porosity of the material.

Guest exchange of 2 with hexane and single-crystal-to-single-crystal transformation: When a single crystal of **2** was immersed for three days in *n*-hexane, in which **2** was completely insoluble, the DMF guest molecules in **2** were exchanged with *n*-hexane by retaining the single crystallinity as well as transparency, which provided a single crystal of $\{[Zn_2(BPnDC)_2(dabco)]\cdot 6(n\text{-hexane})\cdot 3H_2O\}_n$ ($\mathbf{2}_{\mathbf{hexane}}$) and thus the X-ray crystal structure of $\mathbf{2}_{\mathbf{hexane}}$ could be determined. The guest exchange was also verified with bulk sample **2** by the elemental analysis, FTIR spectra, and TGA data. TGA data of $\mathbf{2}_{\mathbf{hexane}}$ indicated that *n*-hexane molecules were released as soon as solid $\mathbf{2}_{\mathbf{hexane}}$ was exposed to air, and then water guest molecules were removed on heating to approximately 140 °C. As shown in Figure 6, the simulated PXRD pattern for $\mathbf{2}_{\mathbf{hexane}}$ is coincident with that of the simulated pattern for **2**, even though the measured PXRD pattern of $\mathbf{2}_{\mathbf{hexane}}$ shows the broadened peaks because $\mathbf{2}_{\mathbf{hexane}}$ loses *n*-hexane as soon as it is exposed to air. After exposure of $\mathbf{2}_{\mathbf{hexane}}$ to air for a few minutes, the PXRD pattern becomes different from either the measured or the simulated pattern for $\mathbf{2}_{\mathbf{hexane}}$, which indicates that the framework structure changes upon removal of the guest molecules. The PXRD pattern measured for completely dried solid of $\mathbf{2}_{\mathbf{hexane}}$ is very similar to that of **2′**. In addition, the PXRD pattern of $\mathbf{2}_{\mathbf{hexane}}$ could not be regenerated even when desolvated solid of $\mathbf{2}_{\mathbf{hexane}}$ was immersed in *n*-hexane for two days, thus indicating that the original structure can hardly be restored once the guest molecules are removed. Desolvated solid of $\mathbf{2}_{\mathbf{hexane}}$ does not adsorb N_2 or H_2 gas.

The X-ray data quality of $\mathbf{2}_{\mathbf{hexane}}$ was as good as that of **2**. The cell parameters including the cell volume of $\mathbf{2}_{\mathbf{hexane}}$ are almost the same as those of **2**, but the crystal space group changes to $I4_1/a$ compared with $I4_1/amd$ of **2** (Table 2). The framework structure of $\mathbf{2}_{\mathbf{hexane}}$ is compared with that of **2** in

Table 2. Crystallographic data for **1**, **2**, and $\mathbf{2}_{\mathbf{hexane}}$ (squeezed data).

	1	**2**	$\mathbf{2}_{\mathbf{hexane}}$
formula	$Cu_2C_{40}H_{24}N_2O_{10}$	$Zn_2C_{36}H_{28}N_2O_{10}$	$Zn_2C_{36}H_{28}N_2O_{10}$
space group	$I4_1/amd$	$I4_1/amd$	$I4_1/a$
M_r	819.73	779.39	779.39
a [Å]	28.000(1)	19.423(1)	19.451(1)
c [Å]	43.969(1)	50.966(1)	50.918(1)
V [Å^3]	34472(2)	19226(1)	19263(1)
Z	8	8	8
ρ_{calcd} [g cm^{-3}]	0.316	0.539	0.537
T [K]	293(2)	293(2)	293(2)
μ [mm^{-1}]	0.260	0.521	0.520
GOF (F^2)	0.844	0.878	0.886
R_1, wR_2	0.0777[a],	0.0929[a],	0.0955[a],
$[I>2\sigma(I)]$	0.1839[b]	0.2283[c]	0.2479[d]
R_1, wR_2 (all	0.1958[a],	0.1702[a],	0.1527[a],
data)	0.2070[b]	0.2533[c]	0.2733[d]

[a] $R=\Sigma||F_o|-|F_c||/\Sigma|F_o|$. [b] $wR(F^2)=[\Sigma w(F_o^2-F_c^2)^2/\Sigma w(F_o^2)^2]^{1/2}$ in which $w=1/[\sigma^2(F_o^2)+(0.0917P)^2+(0.00)P]$, $P=(F_o^2+2F_c^2)/3$ for **1**. [c] $wR(F^2)=[\Sigma w(F_o^2-F_c^2)^2/\Sigma w(F_o^2)^2]^{1/2}$ in which $w=1/[\sigma^2(F_o^2)+(0.1331P)^2+(0.00)P]$, $P=(F_o^2+2F_c^2)/3$ for **2**. [d] $wR(F^2)=[\Sigma w(F_o^2-F_c^2)^2/\Sigma w(F_o^2)^2]^{1/2}$ in which $w=1/[\sigma^2(F_o^2)+(0.1579P)^2+(0.00)P]$, $P=(F_o^2+2F_c^2)/3$ for $\mathbf{2}_{\mathbf{hexane}}$.

Figure 5. The local structures of the Zn_2 paddle-wheel unit and $BPnDC^{2-}$ ligands are very similar to those of **2**. However, the Zn_2 paddle-wheel unit and $BPnDC^{2-}$ ligand undergo positional and rotational rearrangements upon guest exchange. In particular, dihedral angles between the carboxylate planes forming the paddle-wheel SBUs and the linking phenyl rings become 9.02(1.17) and 4.39(1.03)° in $\mathbf{2}_{\mathbf{hexane}}$, compared with 2.42(1.22)° in **2**. In addition, the dihedral angle between the two phenyl rings of a $BPnDC^{2-}$ moiety changes to 57.04(27)° from 59.02(25)° in **2**. As a result, the four carboxylate carbon atoms of each paddle wheel perform a bending motion, and the dihedral angle between the square planes of the paddle-wheel units becomes 50.84(23)°, which is remarkably different from that in **2** (89.97(1)°). Furthermore, a dabco ligand occupying the axial site of Zn^{II} ion is slightly more tilted with respect to the Zn–Zn axis (N-Zn-Zn: 174.08(10)° in $\mathbf{2}_{\mathbf{hexane}}$ versus 177.54(13)° in **2**). This type of guest-responsive single-crystal-to-single-crystal transformation that involves the movements of molecular components can be applied in the development of devices and sensors.

Conclusion

We have prepared two isomorphous 3D metal–organic frameworks generating 2D channels, $\{[Cu_2(BPnDC)_2(bpy)]\cdot 8DMF\cdot 6H_2O\}_n$ (**1**) and $\{[Zn_2(BPnDC)_2(dabco)]\cdot 13DMF\cdot 3H_2O\}_n$ (**2**). MOFs **1** and **2** have large pores with effective sizes of 18.2 and 11.4 Å, respectively. The desolvated framework of **1** (**SNU-6**) exhibits high permanent porosity (1.05 cm^3 g^{-1}) with high Langmuir surface area (2910 m^2 g^{-1}), high H_2 storage capacity (1.68 wt% at 77 K and 1 atm; excess 4.87 wt% and total 10.0 wt% at 77 K and 70 bar), and high CO_2 uptake capability (113.8 wt% at 195 K and 1 atm). When the DMF guest molecules in **2** are exchanged with *n*-hexane, **2** undergoes a single-crystal-to-single-crystal transformation to result in $\{[Zn_2(BPnDC)_2(dabco)]\cdot 6(n\text{-hexane})\cdot 3H_2O\}_n$ ($\mathbf{2}_{\mathbf{hexane}}$). The X-ray crystal structure of $\mathbf{2}_{\mathbf{hexane}}$ indicates that the guest exchange induces mainly a bending motion of the square planes of the paddle-wheel units, which results from the rotational rearrangements of phenyl rings and carboxylate planes of $BPnDC^{2-}$. The present study suggests that solid **SNU-6** can be applied in storage of H_2 and CO_2 gases as well as separation of CO_2 versus CH_4 gas. Solid **2** can be applied in the development of crystalline devices and sensors.

Experimental Section

General methods: All chemicals and solvents used in the syntheses were of reagent grade and used without further purification. Infrared spectra were recorded with a Perkin-Elmer Spectrum One FTIR spectrophotometer. UV/Vis spectra were recorded with a Perkin-Elmer Lambda35 UV/Vis spectrophotometer. Elemental analyses were performed with a Perkin-Elmer 2400 Series II CHN analyzer. Thermogravimetric analysis (TGA) and differential scanning calorimetry (DSC) were performed under an N_2 atmosphere at a scan rate of 5 °C min^{-1}, using TGA Q50 and DSC Q10 of TA instruments, respectively. Powder X-ray diffraction (PXRD) data were recorded on a Bruker D5005 diffractometer at 40 kV and 40 mA for $Cu_{K\alpha}$ ($\lambda=1.54050$ Å) with a scan speed of 5° min^{-1} and a step size of 0.02° in 2θ.

Preparation of $\{[Cu_2(BPnDC)_2(bpy)]\cdot 8DMF\cdot 6H_2O\}_n$ (1): H_2BPnDC (0.056 g, 2.1×10^{-4} mol) and 4,4′-bpy (0.018 g, 1.2×10^{-4} mol) were dissolved in DMF (6 mL), and $Cu(NO_3)_2\cdot 2.5H_2O$ (0.061 g, 3.3×10^{-4} mol) was dissolved in EtOH (3 mL). The solutions were mixed together, placed in a glass serum bottle that was tightly capped with a silicone stopper and aluminum seal, and then heated at 80 °C for 24 h. On cooling to room temperature, blue diamond-shaped crystals formed, which were filtered, and washed briefly with DMF. Yield: 0.13 g, 82%; FTIR (Nujol): $\tilde{\nu}=3436$ (O–H), 1667 (br; C=O(DMF), C=O(BPnDC)), 1628 (C=O), 1608 (C=C(aromatic)), 1559 cm^{-1} (O–C=O (carboxylate)); UV/Vis (diffuse reflectance): $\lambda_{max}=272$, 745 nm; elemental analysis calcd (%) for $Cu_2C_{64}H_{92}O_{24}N_{10}$: C 50.82, H 6.13, N 9.26; found: C 51.04, H 5.60, N 9.17.

Preparation of $[Cu_2(BPnDC)_2(bpy)]_n$ (SNU-6): Compound **1** was heated in a Schlenk tube at 100 °C under vacuum for 2 h. FTIR (Nujol): $\tilde{\nu}=$ 1668, 1631 (C=O), 1606 (C=C(aromatic)), 1561 cm^{-1} (O–C=O(carboxylate)); UV/Vis (diffuse reflectance): $\lambda_{max}=272$, 735 nm; elemental analysis calcd (%) for $Cu_2C_{40}H_{24}O_{10}N_2$: C 58.61, H 2.95, N 3.42; found: C 57.48, H 2.87, N 3.20.

Preparation of $\{[Zn_2(BPnDC)_2(dabco)]\cdot 13DMF\cdot 3H_2O\}_n$ (2): H_2BPnDC (0.053 g, 2.0×10^{-4} mol) and dabco (0.015 g, 1.3×10^{-4} mol) were dissolved in DMF (3 mL), and $Zn(NO_3)_2\cdot 6H_2O$ (0.077 g, 2.6×10^{-4} mol) was dissolved in DMF (2 mL). The solutions were mixed together, placed in a glass serum bottle that was tightly capped with a silicone stopper and aluminum seal, and then heated at 100 °C for 3 d. On cooling to room temperature, colorless diamond-shaped crystals formed, which were filtered, and washed briefly with DMF. Yield: 0.12 g, 67%; FTIR (Nujol): $\tilde{\nu}=$ 3436 (O–H), 2952, 2924, 2854 (C–H(aliphatic)), 1665 (br; C=O(DMF), C=O(BPnDC)), 1604 (C=C(aromatic)), 1541 cm^{-1} (O–C=O(carboxylate)); elemental analysis calcd (%) for $Zn_2C_{75}H_{125}O_{26}N_{15}$: C 50.50, H 7.06, N 11.78; found: C 50.71, H 6.87, N 11.78.

Preparation of $[Zn_2(BPnDC)_2(dabco)]_n$ (2′): Compound **2** was heated in a Schlenk tube at 100 °C under vacuum for 2 h. FTIR (Nujol): $\tilde{\nu}=1638$ (C=O), 1600 (C=C(aromatic)), 1549 cm^{-1} (O–C=O(carboxylate)); elemental analysis calcd (%) for $Zn_2C_{36}H_{28}O_{10}N_2$: C 55.48, H 3.62, N 3.59; found: C 54.13, H 4.13, N 3.54.

Preparation of $\{[Zn_2(BPnDC)_2(dabco)]\cdot 6(n\text{-hexane})\cdot 3H_2O\}_n$ ($\mathbf{2}_{\mathbf{hexane}}$): Crystals of **2** were immersed in *n*-hexane for 24 h, and then the solvent was discarded. Fresh *n*-hexane was added and the crystals were left im-

mersed for another 2 d until all the DMF guest molecules were exchanged with *n*-hexane. FTIR (Nujol): $\tilde{\nu}=1642$ (C=O), 1610, 1554 cm^{-1} (O−C=O(carboxylate)); elemental analysis calcd (%) for $Zn_2C_{72}H_{118}O_{13}N_2$: C 62.70, H 8.29, N 2.22; found: C 62.49, H 7.80, N 2.19.

Low-pressure gas sorption measurements: The gas adsorption–desorption experiments were performed by using an automated micropore gas analyzer Autosorb-1 or Autosorb-3B (Quantachrome Instruments). The crystals of **1** as synthesized were directly introduced into the gas sorption apparatus, and the outgassing process was carried out by heating the sample at 100 °C under vacuum for 2 h. All gases used were of 99.999 % purity. The H_2 gas sorption isotherms were monitored at 77 and 87 K, and CO_2 and CH_4 gas sorption isotherms were measured at both 195 and 273 K, at each equilibrium pressure by the static volumetric method. After each gas sorption measurement, sample weight was measured again precisely. Surface area and total pore volume were determined from the N_2 gas isotherm at 77 K. For multipoint BET and Langmuir surface area estimations, the data were taken in the range of $P/P_0=0.004$–0.05 and $P/P_0=0.002$–0.08, respectively.

High-pressure H_2 gas sorption measurements: The high-pressure H_2 sorption isotherm of **SNU-6** was measured at 77 K in the range of 0–70 bar by the gravimetric method using a Rubotherm MSB (magnetic suspension balance) apparatus. Solid **1** was heated in a Schlenk tube at 100 °C under vacuum for 2 h, and an exactly measured amount of the dried solid was introduced into the gas sorption apparatus, which was then evacuated at 25 °C under vacuum. All data were corrected for the buoyancy of the system and sample. The sample density used in the buoyancy correction was determined from He displacement isotherms (up to 80 bar) measured at 298 K.

Single-crystal-to-single-crystal transformation study for guest exchange of 2 with hexane: A crystal of **2** was sealed in a glass capillary with the mother liquor. After the diffraction data of the crystal were collected, the crystal was taken out from the capillary and then dropped into a 1.5 mL vial that was filled with *n*-hexane. After immersion in *n*-hexane for 3 d, the crystal was sealed in a glass capillary together with *n*-hexane and mounted on a X-ray diffractometer.

X-ray crystallography: Diffraction data of **1**, **2**, and $\mathbf{2_{hexane}}$ were collected on an Enraf Nonius Kappa CCD diffractometer with graphite-monochromated $Mo_{K\alpha}$ radiation ($\lambda=0.71073$ Å) at 293 K. The single crystals of **1**, **2**, and $\mathbf{2_{hexane}}$ were sealed in a glass capillary together with the mother liquor. Preliminary orientation matrixes and unit cell parameters were obtained from the peaks of the first ten frames and then refined using the whole data set. Frames were integrated and corrected for Lorentz and polarization effects by using DENZO.[54] The scaling and global refinement of crystal parameters were performed by SCALEPACK.[54] No absorption correction was made. The crystal structure was solved by direct methods[55] and refined by full-matrix least-squares refinement using the SHELXL-97 computer program.[56] For **1**, two carbon atoms of 4,4′-bpy were rotationally disordered twofold. The site occupancy factors were given as 0.5 for C9A, C9B, C10A, and C10B. The positions of all non-hydrogen atoms were refined with anisotropic displacement factors. The hydrogen atoms were positioned geometrically by using a riding model. The densities of the disordered guest molecules in **1**, **2**, and $\mathbf{2_{hexane}}$ were flattened by using the SQUEEZE option of PLATON.[40] CCDC-689694 (**1**), 689695 (**2**), and 689696 ($\mathbf{2_{hexane}}$) contain the supplementary crystallographic data for this paper. These data can be obtained free of charge from The Cambridge Crystallographic Data Centre via www.ccdc.cam.ac.uk/data_request/cif. The crystallographic data for **1**, **2**, and $\mathbf{2_{hexane}}$ are summarized in Table 2.

Acknowledgements

This work was supported by a Korea Research Foundation grant (Basic Research Promotion Fund, KRF-2005-084-C00020), and by a Korea Science and Engineering Foundation grant (KOSEF, R11-2005-008-00000-0) funded by the Korean government (MEST).

[1] Y. E. Cheon, M. P. Suh, *Chem. Eur. J.* **2008**, *14*, 3961–3967.
[2] B. Chen, S. Ma, F. Zapata, F. R. Fronczek, E. B. Lobkovsky, H.-C. Zhou, *Inorg. Chem.* **2007**, *46*, 1233–1236.
[3] J. W. Yoon, S. H. Jhung, Y. K. Hwang, S. M. Humphrey, P. T. Wood, J.-S. Chang, *Adv. Mater.* **2007**, *19*, 1830–1834.
[4] M. P. Suh, Y. E. Cheon, E. Y. Lee, *Chem. Eur. J.* **2007**, *13*, 4208–4215.
[5] B. Chen, C. Liang, J. Yang, D. S. Contreras, Y. L. Clancy, E. B. Lobkovsky, O. M. Yaghi, S. Dai, *Angew. Chem.* **2006**, *118*, 1418–1421; *Angew. Chem. Int. Ed.* **2006**, *45*, 1390–1393.
[6] H. R. Moon, N. Kobayashi, M. P. Suh, *Inorg. Chem.* **2006**, *45*, 8672–8676.
[7] J. A. R. Navarro, E. Barea, J. M. Salas, N. Masciocchi, S. Galli, A. Sironi, C. O. Ania, J. B. Parra, *Inorg. Chem.* **2006**, *45*, 2397–2399.
[8] L. Pan, D. H. Olson, L. R. Ciemnolonski, R. Heddy, J. Li, *Angew. Chem.* **2006**, *118*, 632–635; *Angew. Chem. Int. Ed.* **2006**, *45*, 616–619.
[9] S. S. Kaye, A. Dailly, O. M. Yaghi, J. R. Long, *J. Am. Chem. Soc.* **2007**, *129*, 14176–14177.
[10] M. Latroche, S. Surblé, C. Serre, F. Millange, G. Férey, *Angew. Chem.* **2006**, *118*, 8407–8411; *Angew. Chem. Int. Ed.* **2006**, *45*, 8227–8231.
[11] M. Dinca, A. Dailly, Y. Liu, C. M. Brown, D. A. Neumann, J. R. Long, *J. Am. Chem. Soc.* **2006**, *128*, 16876–16883.
[12] E. Y. Lee, S. Y. Jang, M. P. Suh, *J. Am. Chem. Soc.* **2005**, *127*, 6374–6381.
[13] E. Y. Lee, M. P. Suh, *Angew. Chem.* **2004**, *116*, 2858–2861; *Angew. Chem. Int. Ed.* **2004**, *43*, 2798–2801.
[14] M. J. Manos, R. Iyer, G. E. Quarez, J. H. Liao, M. G. Kanatzidis, *Angew. Chem.* **2005**, *117*, 3618–3621; *Angew. Chem. Int. Ed.* **2005**, *44*, 3552–3555.
[15] H. J. Choi, M. P. Suh, *Inorg. Chem.* **2003**, *42*, 1151–1157.
[16] P. N. Trikalitis, K. K. Rangan, T. Bakas, M. G. Kanatzidis, *J. Am. Chem. Soc.* **2002**, *124*, 12255–12260.
[17] K. S. Min, M. P. Suh, *J. Am. Chem. Soc.* **2000**, *122*, 6834–6840.
[18] C. A. Bauer, T. V. Timofeeva, T. B. Settersten, B. D. Patterson, V. H. Liu, B. A. Simmons, M. D. Allendorf, *J. Am. Chem. Soc.* **2007**, *129*, 7136–7144.
[19] S. Shimomura, R. Matsuda, T. Tsujino, T. Kawamura, S. Kitagawa, *J. Am. Chem. Soc.* **2006**, *128*, 16416–16417.
[20] M. Eddaudi, J. Kim, D. Vodak, A. Sudik, J. Wachter, M. O'Keeffe, O. M. Yaghi, *Proc. Natl. Acad. Sci. U.S.A.* **2002**, *99*, 4900–4904.
[21] H. Chun, D. N. Dybtsev, H. Kim, K. Kim, *Chem. Eur. J.* **2005**, *11*, 3521–3529.
[22] Hydrogen, Fuel Cells, & Infrastructure Technologies Program: Multiyear Research, Development, and Demonstration Plan, U.S. Department of Energy, **2005**, Chapter 3, http://www.eere.energy.gov/hydrogenandfuelcells/mypp/.
[23] A. G. Wong-Foy, A. J. Matzger, O. M. Yaghi, *J. Am. Chem. Soc.* **2006**, *128*, 3494–3495.
[24] Y. Li, R. Yang, *Langmuir* **2007**, *23*, 12937–12944.
[25] A. R. Millward, O. M. Yaghi, *J. Am. Chem. Soc.* **2005**, *127*, 17998–17999.
[26] M. P. Suh, J. W. Ko, H. J. Choi, *J. Am. Chem. Soc.* **2002**, *124*, 10976–10977.
[27] H. J. Choi, M. P. Suh, *J. Am. Chem. Soc.* **2004**, *126*, 15844–15851.
[28] M. P. Suh, H. R. Moon, E. Y. Lee, S. Y. Jang, *J. Am. Chem. Soc.* **2006**, *128*, 4710–4718.
[29] M. P. Suh, Y. E. Cheon, *Aust. J. Chem.* **2006**, *59*, 605–612.
[30] O. Ohmori, M. Kawano, M. Fujita, *Angew. Chem.* **2005**, *117*, 1998–2000; *Angew. Chem. Int. Ed.* **2005**, *44*, 1962–1964.
[31] B. F. Abrahams, M. Moylan, S. D. Orchard, R. Robson, *Angew. Chem.* **2003**, *115*, 1892–1895; *Angew. Chem. Int. Ed.* **2003**, *42*, 1848–1851.
[32] C. D. Wu, W. Lin, *Angew. Chem.* **2005**, *117*, 1994–1997; *Angew. Chem. Int. Ed.* **2005**, *44*, 1958–1961.
[33] S. R. Halper, L. Do, J. R. Stork, S. M. Cohen, *J. Am. Chem. Soc.* **2006**, *128*, 15255–15268.

[34] K. Huang, Z. Xu, Y. Li, H. Zheng, *Cryst. Growth Des.* **2007**, *7*, 202–204.
[35] C. Y. Sun, L. P. Jin, *J. Mol. Struct.* **2006**, *782*, 171–176.
[36] C. Y. Sun, L. P. Jin, *J. Mol. Struct.* **2005**, *733*, 63–68.
[37] H. J. Park, M. P. Suh, unpublished results.
[38] E. B. Rusanov, V. V. Ponomarova, V. V. Komarchuk, H. Stoeckli-Evans, E. Fernandez-Ibanez, F. Stoeckli, J. Sieler, K. V. Domasevitch, *Angew. Chem.* **2003**, *115*, 2603–2605; *Angew. Chem. Int. Ed.* **2003**, *42*, 2499–2501.
[39] H. Chun, J. Moon, *Inorg. Chem.* **2007**, *46*, 4371–4373.
[40] A. L. Spek, PLATON99, A Multipurpose Crystallographic Tool, Utrecht University, Utrecht (The Netherlands), **1999**.
[41] X.-S. Wang, S. Ma, D. Sun, S. Parkin, H.-C. Zhou, *J. Am. Chem. Soc.* **2006**, *128*, 16474–16475.
[42] A. Saito, H. C. Foley, *AIChE J.* **1991**, *37*, 429–436.
[43] Materials Studio program, version 4.1, Accelrys, San Diego, CA, **2006**.
[44] J. L. C. Rowsell, O. M. Yaghi, *J. Am. Chem. Soc.* **2006**, *128*, 1304–1315.
[45] M. Dinca, A. Dailly, C. Tsay, J. R. Long, *Inorg. Chem.* **2008**, *47*, 11–13.
[46] N. A. Ramsahye, G. Maurin, S. Bourrelly, P. L. Llewellyn, T. Loiseau, C. Serre, G. Férey, *Chem. Commun.* **2007**, 3261–3263.
[47] T. K. Maji, R. Matsuda, S. Kitagawa, *Nat. Mater.* **2007**, *6*, 142–148.
[48] K. Uemura, Y. Yamasaki, Y. Komagawa, K. Tanaka, H. Kita, *Angew. Chem.* **2007**, *119*, 6782–6785; *Angew. Chem. Int. Ed.* **2007**, *46*, 6662–6665.
[49] S. Takamizawa, K. Kojima, T. Akatsuka, *Inorg. Chem.* **2006**, *45*, 4580–4582.
[50] S. Bourrelly, P. L. Llewellyn, C. Serre, F. Millange, T. Loiseau, G. Férey, *J. Am. Chem. Soc.* **2005**, *127*, 13519–13521.
[51] R. Kitaura, K. Seki, G. Akiyama, S. Kitagawa, *Angew. Chem.* **2003**, *115*, 444–447; *Angew. Chem. Int. Ed.* **2003**, *42*, 428–431.
[52] K. S. Walton, A. R. Millward, D. Dubbeldam, H. Frose, J. J. Low, O. M. Yaghi, R. Q. Snurr, *J. Am. Chem. Soc.* **2008**, *130*, 406–407.
[53] A. Bondi, *J. Phys. Chem.* **1964**, *68*, 441–451.
[54] Z. Otwinowsky, W. Minor, in *Processing of X-ray Diffraction Data Collected in Oscillation Mode, Methods in Enzymology* (Eds.: C. W. Carter, R. M. Sweet), Academic Press, New York (USA), **1996**, pp. 276, 307–326.
[55] G. M. Sheldrick, *Acta Crystallogr. Sect. A* **1990**, *46*, 467.
[56] G. M. Sheldrick, SHELXL97, Program for the Crystal Structure Refinement, University of Göttingen, Göttingen (Germany), **1997**.

Received: June 2, 2008
Published online: September 12, 2008

